

Cite this: *Lab Chip*, 2011, **11**, 3555

www.rsc.org/loc

## TECHNICAL NOTE

## A biological breadboard platform for cell adhesion and detachment studies†

Sang-Hee Yoon,<sup>‡ab</sup> Jiyoung Chang,<sup>b</sup> Liwei Lin<sup>b</sup> and Mohammad R. K. Mofrad<sup>\*a</sup>

Received 3rd May 2011, Accepted 1st August 2011

DOI: 10.1039/c1lc20369j

The dynamic nature of cell adhesion and detachment, which plays a critical role in a variety of physiological and pathological phenomena, still remains unclear. This motivates the pursuit of controllable manipulation of cell adhesion and detachment for a better understanding of cellular dynamics. Here we present an addressable, multifunctional, and reusable platform, termed the biological breadboard (BBB), for spatiotemporal manipulation of cell adhesion and detachment at cellular and subcellular levels. The BBB, composed of multiple gold electrodes patterned on a Pyrex substrate, is surface-modified with arginine-glycine-aspartic acid terminated thiol (RTT) and polyethylene glycol (PEG) to achieve a cell-adhesive surface on the gold electrodes and a cell-resistive surface on the Pyrex substrate, respectively. Cell adhesion is regulated by the steric repulsion of PEG chains, while cell detachment is controlled by the reductive desorption of a gold-thiol self-assembled monolayer (SAM) at an activation potential of  $-0.90$  to  $-1.65$  V. Experimental characterizations using NIH 3T3 fibroblasts are presented to demonstrate the utility of our device.

## Introduction

Cell adhesion and detachment regulate the behavior and function of adherent cells. Any irregularity in cell adhesion and detachment can potentially lead to various pathophysiological consequences.<sup>1,2</sup> Quantitative characterization of cell adhesion and detachment is therefore essential for understanding disease mechanisms. Yet, little progress has been made in the development of devices that spatiotemporally control cell adhesion and detachment.<sup>3</sup>

The dynamics of cell adhesion and detachment has been studied using various methods. Experimental techniques for cell adhesion manipulation can be classified into photolithography,<sup>4,5</sup> e-beam lithography,<sup>6</sup> dip-pen lithography,<sup>7</sup> nanoimprint lithography,<sup>8</sup> microcontact printing,<sup>9,10</sup> elastomeric stencil,<sup>11</sup> ink-jet printing,<sup>12</sup> optical tweezer,<sup>13</sup> electrophoresis,<sup>14,15</sup> and switchable surface.<sup>16</sup> Although the lithography techniques, microcontact printing, elastomer stencil, and ink-jet printing attempted to manipulate cell adhesion with specific proteins, they were able to

alter cell adhesion only at the beginning of microfabrication and were not involved in manipulating cell detachment. The optical tweezer and electrophoresis were associated with protein denaturation and cell electrolysis, respectively. Experimental techniques for cell detachment manipulation can be categorized into hydrodynamic shear force device,<sup>17–23</sup> centrifugal device,<sup>24–27</sup> and micropipette aspiration.<sup>28–30</sup> Although hydrodynamic shear force device provided reliable characterization of cell detachment with a parallel, rotational, or radial flow, it accompanied the local deformation of cells and the possibility of cell rupture during experiment. The centrifugal device generated a relatively low force for cell detachment, which limited its applications only to cells which were either cultured for short term (less than 1 h) or involved weak cell–substrate interactions. The micropipette aspiration was also used to explore cell adhesion, but the direct contact between cell and micropipette caused cytoskeletal remodeling during experiment. Recently, electrochemical methods for manipulating cell adhesion and detachment have been developed to prevent cell deformation (*e.g.*, protein denaturation, cell electrolysis, direct contact, *etc.*) during experiment. The reductive desorption of a gold-alkanethiol SAM<sup>31</sup> was successful to manipulate cell adhesion only at a cellular level, but involved a relatively complex preparation process. The electrochemical reaction of polyelectrolytes<sup>32</sup> was utilized to control cell adhesion and detachment. However, the multiple depositions of the polyelectrolytes even on cells were thought to change cell behavior, resulting in inaccurate measurements.

A biological breadboard (BBB) is therefore developed to spatiotemporally manipulate cell adhesion and detachment at cellular and subcellular levels. This method, inspired by the electrical breadboard, has the exquisite features of addressability, multifunctionality, reusability, and ease of use: the addressability

<sup>a</sup>Molecular Cell Biomechanics Laboratory, Department of Bioengineering, University of California, Berkeley, California, 94720, USA. E-mail: mofrad@berkeley.edu; Fax: +1-510-642-5835; Tel: +1-510-642-8165

<sup>b</sup>Department of Mechanical Engineering, University of California, Berkeley, California, 94720, USA

† Electronic supplementary information (ESI) available: Biomimetic cell adhesion of BBB (Fig. S1); characterization of two surface modifications by contact angle measurements (Fig. S2); XPS survey spectrum of RTT-functionalized gold surface (Fig. S3); potentiodynamic electrochemical characterization of reductive desorption of gold-thiol SAM (Fig. S4); reusability characterization of BBB (Fig. S5); biochemical reagents for surface modifications (Table S1); videos of cell detachment (Videos S1–5). See DOI: 10.1039/c1lc20369j

‡ Current address: Wyss Institute for Biologically Inspired Engineering, Harvard University, Cambridge, Massachusetts 02138, USA.

of the BBB is due to its independently operated gold electrode array; the BBB can perform a variety of spatiotemporal manipulations on cell adhesion and detachment (*e.g.*, cell patterning (positioning), cell motility control, *etc.*), which makes itself a multifunctional platform for studies of cellular dynamics; the reductive desorption of a gold-thiol SAM secures the BBB's reusability; the BBB can be easily incorporated with other conventional instruments. Moreover, this platform maintains the viability of adherent cells during experiment by mimicking the *in vivo* microenvironment using an arginine-glycine-aspartic acid (RGD) peptide, thus making it possible to characterize the adhesion and detachment of living and intact cells. With this promising technology, we can spatiotemporally control and manipulate cell adhesion and detachment, offering a platform for better understanding of cellular biomechanics.

## Biological breadboard

The BBB consists of identical gold electrodes patterned on a Pyrex substrate, which entitles this platform to a high-degree-of-freedom in manipulating cell adhesion and detachment (Fig. 1A). The gold electrodes are modified with RGD-terminated thiol (RTT) to achieve a cell-adhesive surface. The RGD peptide is tethered to the gold electrodes *via* thiol compound, following the spontaneous chemisorption of  $R-S-H + Au \rightarrow R-S-Au + 1/2H_2$  where R is a substituent.<sup>33</sup> The RGD-ligand is a biomimetic binding site of integrins for cell adhesion (Fig. S1, ESI<sup>†</sup>). The Pyrex substrate is treated with PEG to obtain a cell-resistant surface where hydrated neutral PEG chains sterically prevent cell adhesion.

In the spatiotemporal manipulation of cell adhesion using the BBB modified with RTT and PEG in advance, the RTT on a target area is detached by activating the corresponding gold electrode(s) with a negative potential of  $-0.90$  to  $-1.65$  V, following  $R-S-Au + H^+ + e^- \rightarrow R-S-H + Au$ .<sup>34</sup> This activated platform is sonicated in a cell culture media for 3 min, followed by cell loading. The loaded cells adhere only to the inactivated gold electrodes functionalized with RTT because the RGD peptide of the inactivated gold electrodes has substantially more affinity for cell adhesion than the bare gold of the activated gold electrode(s) (Fig. 1B). The spatiotemporal manipulation of cell detachment is the same as that of cell adhesion except for the order of gold electrode activation and cell loading. In the spatiotemporal manipulation of cell detachment, adherent cells are loaded on the BBB modified with RTT and PEG, and then start to stretch on the RGD peptide of the gold electrodes. On the manipulation of cell detachment, the entire cells (or part of the cell) are detached from the BBB by activating gold electrode(s), breaking a chemical bonding between gold and thiol (Fig. 1C). The detached cells (or part of the cell) sense no external mechanical anchorage (*i.e.*, focal adhesion) to a substrate and undergo gel-sol transition of their cytoskeleton, followed by cellular retraction.

## Materials and methods

### Microfabrication

The microfabrication of the BBB began with a 500  $\mu\text{m}$ -thick, 4-inch, Corning 7740 Pyrex glass wafer. After cleaning the wafer in a piranha solution ( $H_2SO_4 : H_2O_2 = 1 : 1$ ), 1  $\mu\text{m}$ -thick LOR

resist (LOR 10A, MicroChem Corp.) and 2  $\mu\text{m}$ -thick positive photoresist (S1818, Rohm and Haas Corp.) were sequentially spin-coated to prepare a double-layer resist stack for lift-off. This double-layer resist stack was patterned through lithography (Fig. 2A, left), followed by the deposition of 5 nm-thick chromium (Cr) adhesion layer and 100 nm-thick gold (Au) layer through e-beam evaporation (Fig. 2A, center). Next, the Cr/Au layer was patterned in an organic solvent mixture (BAKER PRS-3000 Stripper, Mallinckrodt Baker, Inc.), thus fabricating two kinds of BBBs (Fig. 2A, right). The BBB for the manipulation of cell adhesion and detachment at a cellular level was composed of gold electrodes with a length of 500  $\mu\text{m}$  and a width of 500  $\mu\text{m}$  (Fig. 2B), the other BBB for the manipulation of cell adhesion and detachment at a subcellular level consisted of gold lines with a width of 10  $\mu\text{m}$  and a gap of 3  $\mu\text{m}$  (Fig. 2C). The fabricated BBB was wire-bonded in a chip carrier, and then was assembled with a cell-culture-well (Fig. 2D, left). For the BBB which was used with an inverted microscope, the deposition thickness of the gold layer was reduced to 30 nm to make the BBB transparent (Fig. 2D, right).

### PEG treatment on Pyrex substrate

The fabricated BBB was cleaned with an oxygen plasma chamber (PM-100 Plasma Treatment System, March Plasma Systems, Inc.) at 100 W for 30 s. The cleaned BBB was incubated with 2% v/v m-PEG silane (Gelest, Inc.) and 1% v/v hydrochloric acid (HCl, Fisher Scientific) dissolved in anhydrous toluene (Fisher Scientific) for 2 h (Fig. 2E, left; Table S1, ESI<sup>†</sup>). This treatment was carried out in a glove box under a nitrogen purge. The incubated BBB was sequentially rinsed in fresh toluene and ethanol, followed by drying with nitrogen and curing at 120 °C for 2 h.

### RTT functionalization on gold electrodes

The gold electrodes were functionalized with an RTT solution which was synthesized by chemically combining *cyclo* (Arg-Gly-Asp-D-Phe-Lys) (Peptides International, Inc.) with dithiobis (succinimidyl undecanoate) (Dojindo Molecular Technologies, Inc.) as follows (Table S1, ESI<sup>†</sup>). The *cyclo* (Arg-Gly-Asp-D-Phe-Lys) was dissolved in dimethylsulfoxide (DMSO, Sigma-Aldrich) to get 1 mM RGD peptide aliquot and stored at  $-20$  °C. This reaction was made in a glove box under a nitrogen purge to protect the RGD peptide. The dithiobis(succinimidyl undecanoate) was also prepared in 1 mM aliquot in DMSO and stored at  $-20$  °C. This preparation was also made in moisture-free environment. When functionalizing the gold electrodes, two aliquots were warmed to room temperature in a desiccator. The RGD peptide aliquot was mixed with 1% v/v triethylamine (Fisher Scientific) for 5 min to make all primary amines of a lysine amino acid unprotonated. The same volume of the dithiobis(succinimidyl undecanoate) aliquot was added to the RGD peptide aliquot, and then mixed using a vortex mixer for 4 h to synthesize an RTT solution. For the RTT functionalization of the gold electrodes (Fig. 2E, right), the PEG-treated BBB was incubated with this solution for 1 h at room temperature to promote spontaneous chemisorption between thiol and gold,

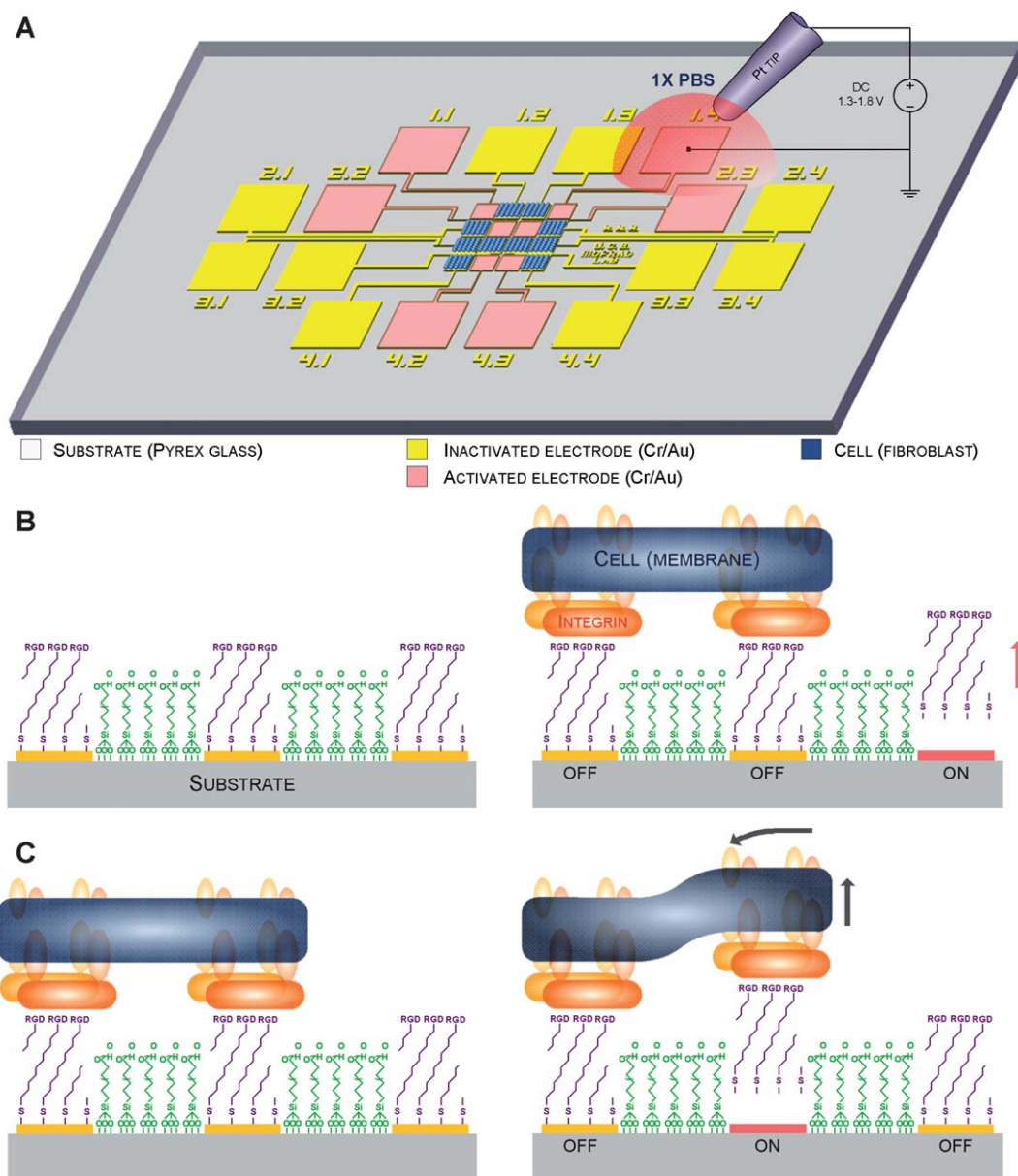


**Fig. 1** A biological breadboard for the spatiotemporal manipulation of cell adhesion and detachment at cellular and subcellular levels. (A) Schematic of the BBB consisting of gold electrodes patterned on a Pyrex substrate. This platform has the addressability, multifunctionality, and reusability in cell manipulation due to its structure and working principle. (B) Cell adhesion manipulation using the BBB. All gold electrodes are functionalized with RTT to induce cell adhesion, whereas the Pyrex substrate is treated with PEG to prevent cell adhesion (left). Before cell loading, the RGD peptides on a target electrode (third electrode from left) are detached by activating the target electrode, followed by cell loading (right). The loaded cell adheres only to inactivated gold electrodes (first and second ones from left). (C) Cell detachment manipulation using the BBB. A cell adheres to all gold electrodes functionalized with RTT (left). The cell (or part of the cell) is detached when a target electrode (second one from left) is activated by applying an activation potential which reductively desorbs a gold-thiol SAM.

followed by sonicating in DMSO for 3 min and rinsing in ethanol and phosphate buffered saline (PBS, Sigma-Aldrich).

#### Contact angle measurement

The contact angles of two surfaces (*i.e.*, PEG-treated Pyrex substrate and RTT-functionalized gold surface) were measured in a sessile drop mode using a goniometer (KRÜSS582, KRÜSS) to characterize the changes in wetting properties of the surfaces through surface modifications. The contact angle of each surface

was measured 10 times, and then was averaged. The contact angle of PEG-treated Pyrex substrate was compared to that of untreated Pyrex substrate, and the contact angle of RTT-functionalized gold surface was compared to those of untreated gold surface and thiol-treated gold surface.

#### X-ray photoelectron spectroscopy (XPS) characterization

A sample for XPS characterization was prepared by performing the RTT functionalization on a Cr/Au layer patterned on

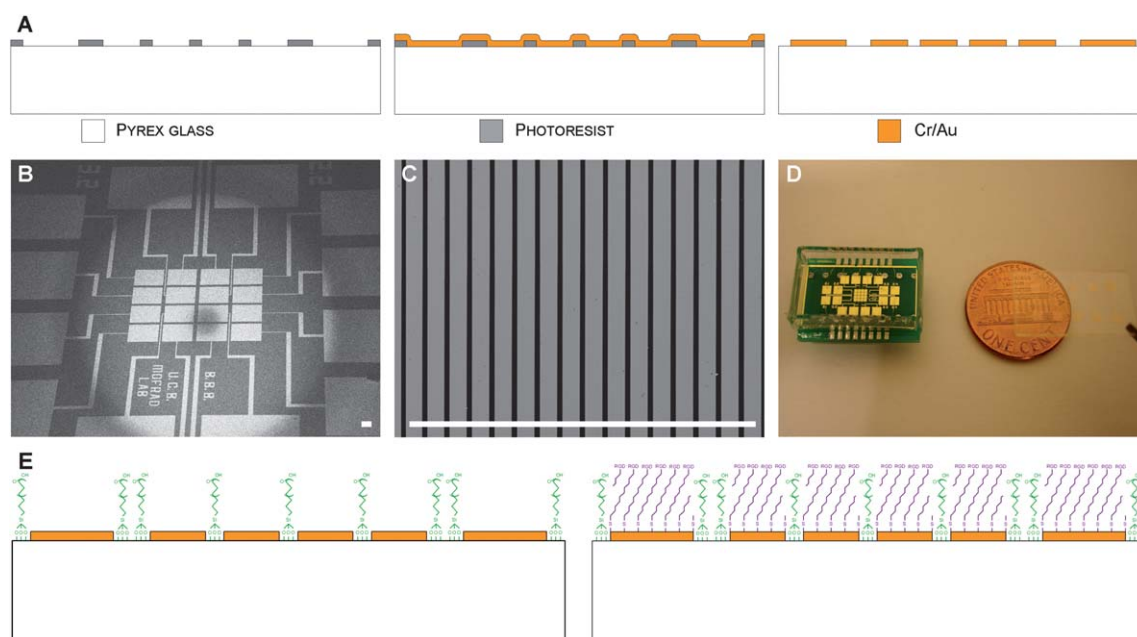


**Fig. 2** Microfabrication and surface modifications of the BBB. (A) The BBB is microfabricated by patterning gold electrodes on a Pyrex substrate: patterning of a photoresist layer through lithography (left); deposition of a Cr/Au layer through e-beam evaporation (center); patterning of the deposited Cr/Au layer through lift-off process (right). (B) Microfabricated BBB for the manipulation of cell adhesion and detachment at a cellular level, each electrode of which is 500  $\mu\text{m}$  in length and 500  $\mu\text{m}$  in width. (C) Microfabricated BBB for the subcellular manipulation, each electrode of which is 10  $\mu\text{m}$  in width and 3  $\mu\text{m}$  in gap. (D) Photograph of the BBB before (right) and after (left) assembly, showing its transparency. (E) Surface modification processes of the BBB. The BBB is incubated with a PEG solution to make a Pyrex substrate cell-resistant (left), and then it is incubated with a synthesized RTT solution to make the gold electrodes cell-adhesive (right). Scale bars of (B) and (C) are 100  $\mu\text{m}$ .

a silicon wafer. An untreated gold pattern was run as a control group. The XPS analysis was conducted using a customized ESCA (Omicron NanoTechnology) at  $1 \times 10^{-8}$  Torr. All measured spectra were referenced to the position of Au 4f peak. The scans were collected over a range of 20 eV around the peak of interest with a pass energy of 23.5 eV.

#### Potentiodynamic electrochemical characterization of reductive desorption of gold-thiol SAM

A Cr/Au layer patterned on a silicon wafer was functionalized in the RTT solution to prepare the sample for cyclic voltammetry characterization. The potentiodynamic electrochemical characterization was performed using a three-electrode system composed of the gold surface of the sample (working electrode), platinum electrode (counter electrode), and Ag/AgCl electrode (reference electrode). The cyclic voltammetry of the reductive desorption of a gold-thiol SAM was measured in Dubecco's phosphate buffered saline (DPBS, Sigma-Aldrich) using a scanning potentiostat (Model 362, EG&G Co.). A scan started cathodically from 0 to  $-2$  V, then anodically back to 0 V at a scan rate of 50  $\text{mV s}^{-1}$ .

#### Cultivation and loading of NIH 3T3 fibroblasts

NIH 3T3 mouse embryonic fibroblast cells (NIH 3T3 fibroblasts) were cultured in Dulbecco's modified eagle medium (DMEM, GIBCO™) supplemented with 10% fetal bovine serum (FBS, GIBCO™) and 1% Penicillin-Streptomycin (Pen-Strep, GIBCO™) at 37 °C in humidified 5%  $\text{CO}_2$  atmosphere. The cell

was passaged every four days. NIH 3T3 fibroblasts with a passage number of 5 to 20 were used in this study. For each experiment, the surface-modified BBB was sterilized, and then was placed on a Petri dish containing 5 ml cell culture medium with a cell suspension of  $1 \times 10^6$  cells/ml. For subcellular detachment, the cell concentration was changed into  $1 \times 10^4$  cells/ml. Unadhered cells were removed by washing the BBB in PBS 1 h after cell loading. All experiments were carried out 24 h after cell loading.

#### Immunofluorescence microscopy

Cells were washed with PBS and fixed in 4% formaldehyde (Fisher Scientific) solution in chilled PBS for 15 min. After fixation, the cells were washed with PBS and then treated with 0.5% Triton X-100 (Sigma-Aldrich) in PBS for 10 min and blocking solution (1% bovine serum albumin (BSA, Fisher Scientific) in PBS) for 1 h. To visualize actin filaments, the cells were treated with rhodamine phalloidin (Biotium, Inc.) diluted 1 : 20 in the blocking solution for 20 min. For nucleus staining, ProLong® gold antifade reagent with DAPI (Invitrogen) was added into the cells.

#### Characterization of viability of detached cells

The viability of detached NIH 3T3 fibroblasts was tested by examining the growth of the cells using the live/dead viability/cytotoxicity assay kit (Invitrogen). The cells detached from the BBB were collected and seeded on a 6-well cell culture plate. After incubating the cells for 24 h, 50  $\mu\text{l}$  of the combined

live/dead cell staining solution (2  $\mu\text{M}$  calcein AM and 4  $\mu\text{M}$  EthD-1 in DPBS) was added to each well, and was incubated with the cells for 30 min at room temperature. Images were obtained using a fluorescent microscope (Axiovert 200, Carl Zeiss MicroImaging, Inc.).

## Results and discussion

The degree of PEG treatment on Pyrex substrate was verified by both contact angle measurement and cell loading test. The measured contact angle of the PEG-treated Pyrex substrate was  $61.5 \pm 3.8^\circ$  on average, while that of untreated Pyrex substrate was  $25.7 \pm 1.5^\circ$  (Fig. S2A, ESI†). Additionally, NIH 3T3 fibroblasts were seeded on both surfaces, and then cell adhesion to each surface was visualized 24 h after cell loading (Fig. S2B, ESI†). These results show the PEG treatment makes the Pyrex substrate strongly hydrophobic, thus effectively preventing cell adhesion.

The RTT functionalization on gold surface was characterized by both contact angle measurement and XPS survey. The average contact angles measured from untreated gold surface, thiol-treated gold surface, and RTT-functionalized gold surface were  $67.3 \pm 2.5^\circ$ ,  $53.3 \pm 1.3^\circ$ , and  $24.6 \pm 2.8^\circ$ , respectively (Fig. S2C, ESI†). The existence of RGD peptides tethered to the gold electrodes was also investigated using XPS. The measured XPS survey spectrum shows the presence of gold, thiol, and RGD peptides (Fig. S3, ESI†): the peaks of Au 4s, Au 4p, Au 4d, and Au 4f indicate the presence of gold (Au(111)); the peaks of S 2p<sub>1/2</sub> and S 2p<sub>3/2</sub> are corresponding to sulfur from the thiol (right inset); the peaks of C 1s, O 1s, O KLL, and N 1s (left inset) demonstrate there are carbon, oxygen, and nitrogen from the amine (–NH<sub>2</sub>) and carboxylic (–COOH) groups of the RGD peptides. Together with the results of contact angle measurements, this confirms RGD-peptides are well linked to the gold electrodes *via* thiol through RTT functionalization.

The reductive desorption of a gold-thiol SAM was verified by measuring cyclic voltammetry (CV) curves using a three-electrode system (Fig. S4A, ESI†). The current at the working electrode (gold electrode of the BBB) was plotted *versus* the applied voltage with respect to a reference electrode (Fig. S4B, ESI†). The part of the CV (*sec. I*) ranging from 0.00 to  $-0.90$  V was

corresponding to no reductive desorption of the SAM; the potential range (*sec. II*) showed the deductive desorption began and ended at  $-0.90$  V (point a) and  $-1.65$  V (point c), respectively; this electrochemical reaction was maximized at  $-1.50$  V (point b). This measurement shows the activation potential must be larger than  $-0.90$  V to break the chemical binding between gold and thiol. Considering the generation of hydrogen due to the electrolysis of cell culture medium at around  $-2.00$  V, the optimum potential for the reductive desorption of a gold-thiol SAM is thought to be  $-1.00$  (larger than  $-0.90$  V) to  $-1.80$  V (less than  $-2.00$  V) at which NIH 3T3 fibroblasts are successfully detached from the gold electrode of the BBB without viability (described later in detail).

The adhesion of adherent cells (NIH 3T3 fibroblasts) was spatiotemporally manipulated using a surface-modified BBB composed of two-by-one gold electrodes. Before cell loading, the left (or bottom) electrode of the BBB was activated (without RGD peptides), but the right (or top) electrode was inactivated (with RGD peptides). When NIH 3T3 fibroblasts were loaded on the BBB with cell concentrations of  $1 \times 10^4$  (Fig. 3A) and  $1 \times 10^6$  cells ml<sup>-1</sup> (Fig. 3B), the cells adhered only to the right electrode because the RGD peptides of the inactivated electrode had much higher affinity for cell adhesion than the bare gold of the activated electrode. This shows the BBB can manipulate cell adhesion in an addressable manner.

The spatiotemporal manipulation of cell detachment at a cellular level was characterized by disconnecting entire living cell(s) from the gold electrodes of the BBB. The biological characterization was conducted at  $-1.5$  V for two NIH 3T3 fibroblasts (Fig. 4A, Video S1, ESI†), subconfluent cells with 25% confluence (Fig. 4B, Video S2, ESI†), subconfluent cells with 50% confluence, subconfluent cells with 75% confluence, and confluent cells with 100% confluence (Fig. 4C). As an evaluation index for the speed of cell detachment at a cellular level, a time required to detach 95% of the adhered cells (CD-time) was measured. The CD-times of the above five cases (averaged from at least 10 measurements) were  $45.2 \pm 6.8$ ,  $36.7 \pm 8.7$ ,  $31.1 \pm 4.2$ ,  $24.8 \pm 5.5$ , and  $21.1 \pm 3.5$  s, respectively (Fig. 4D), showing an inverse proportion to cell confluence. This is because the detachment of a cell applies additional vertical force to neighboring cells through cell–cell interactions at confluent conditions

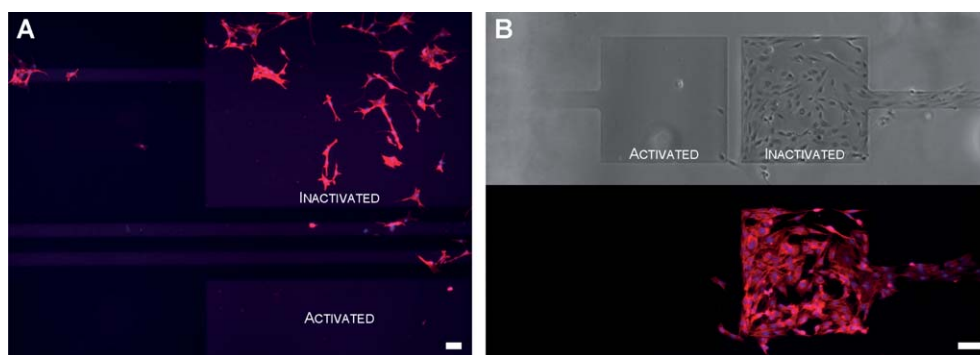


**Fig. 3** Spatiotemporal manipulation of cell adhesion using the BBB. (A) Immunofluorescence image when cell confluence is about 25%. The bottom gold electrode is activated, whereas the top one is inactivated. The NIH 3T3 fibroblasts are stained for actin filaments with rhodamine phalloidin (red) and for a nucleus with DAPI (blue). (B) Immunofluorescence and optical images when cell confluence is about 100%. The left electrode is activated, while the right one is inactivated. These images show the BBB is able to spatiotemporally manipulate cell adhesion. Scale bars are 100  $\mu\text{m}$ .

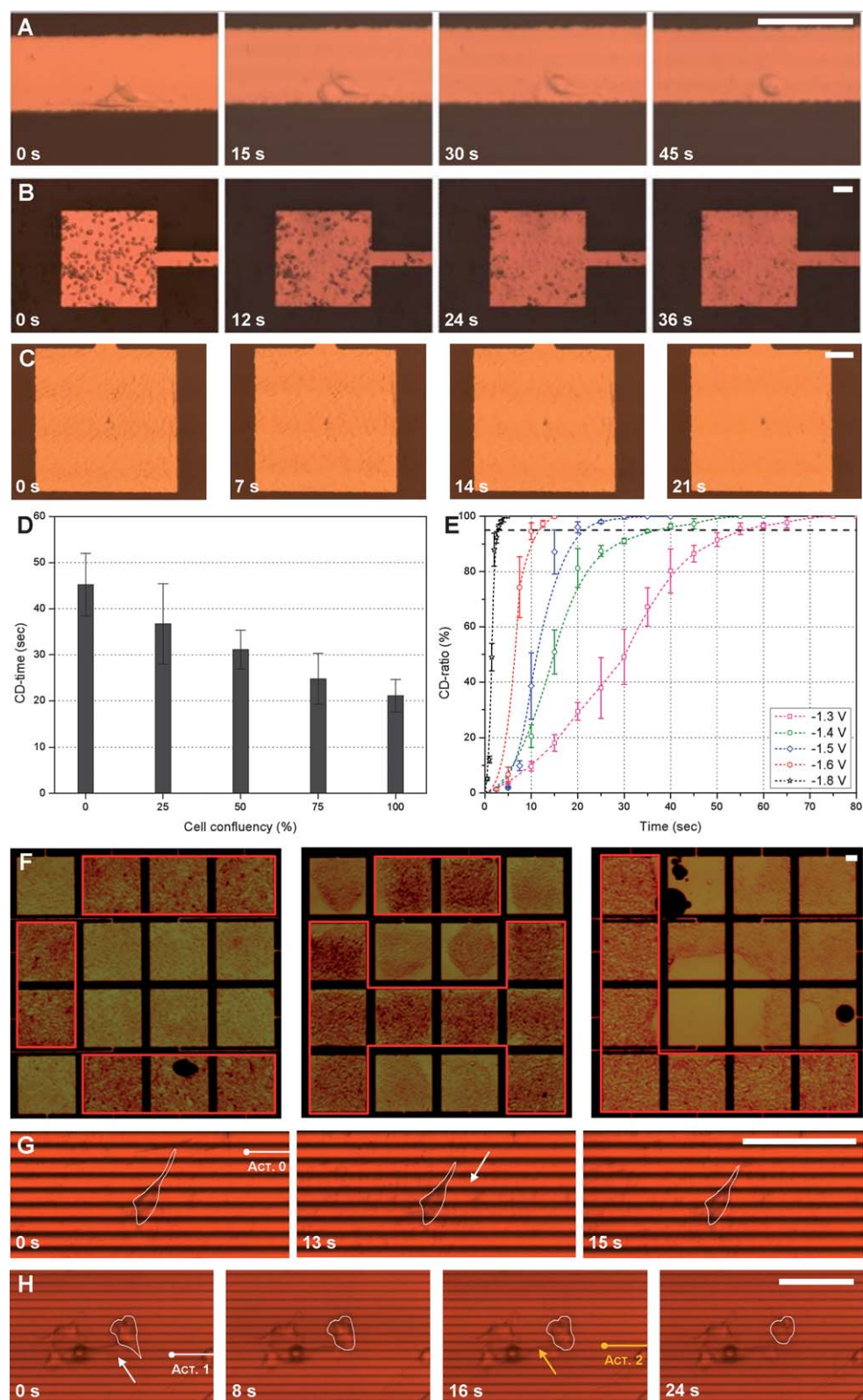


**Fig. 4** Spatiotemporal manipulation of cell detachment using the BBB. (A–C) Optical sequential images showing the spatiotemporal manipulation of cell detachment at a cellular level for two cells (0% confluent cells), 25% confluent cells, and 100% confluent cells. The two cells are detached from a gold electrode at an activation potential of  $-1.5$  V, and their CD-time is  $45.2 \pm 6.8$  s (A). The average CD-time of the 25% confluent cells is  $36.7 \pm 8.7$  s (B). The average CD-time of the 100% confluent cells is  $21.1 \pm 3.5$  s. (D) Measured CD-time as a function of cell confluence. This shows the CD-time is in inverse proportion to cell confluence. (E) Measured CD-ratio as a function of time and activation potential for 100% confluent cells. The CD-ratio is monotonically increasing with two inflection points (s-shaped curve), indicating there is a large deviation in the strength of integrin binding to

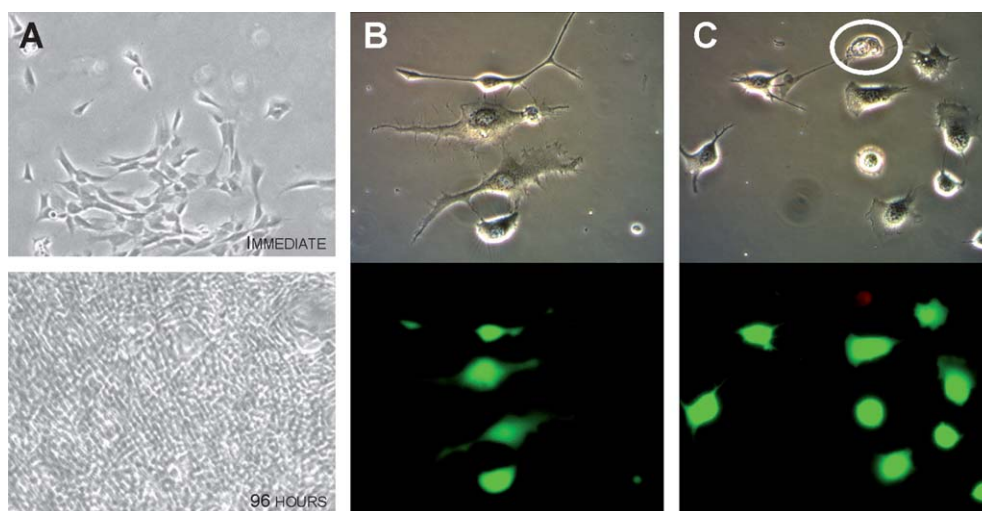


**Fig. 5** Characterization of the viability of cells adhered/detached to/from the BBB. (A) Optical images of NIH 3T3 fibroblasts on inactivated gold electrodes immediately after activation (top) and 96 h after activation (bottom). The cells are normally grown to their confluent stage. (B–C) Optical and immunofluorescence images of cells which are detached from the BBB and then were cultured in a Petri dish for 12 h. All cells detached at an activation potential of  $-1.50$  V are still alive rather than electrocuted (B). About 90% of the cells detached at  $-1.80$  V are alive (C). Viable and dead cells are shown in green and red, respectively. These results show the viability of adherent cells manipulated by the BBB is almost insensitive to the reductive desorption of a gold-thiol SAM (when the activation potential is less than  $-2.00$  V).

where all cells are connected to each other by the cell–cell interactions. This measurement indicates cell–cell interactions have a correlation to cell detachment behavior. The dependence of cell detachment on an activation potential was also investigated by counting the ratio of detached cells to total cells (CD-ratio) as a function of time and activation potential (Fig. 4E, Videos S3–S5, ESI†). The CD-ratio increased as the activation potential increased because the reductive desorption of a gold-thiol SAM was in direct proportion to the activation potential (see Fig. S4B, ESI†). The measured CD-ratio was monotonically increasing with two inflection points (s-shape curves), demonstrating a large deviation in the strength of integrin binding to extracellular matrix proteins or another cell. A programmable cell patterning was also performed. A single four-by-four BBB was used to spatiotemporally manipulate the detachment of NIH 3T3 fibroblasts at a cellular level (Fig. 4F). That is, the cells were sequentially patterned in a shape of “C,” “A,” or “L” using the BBB, and then the BBB was reused for the next cell patterning after cleaning it (Fig. S5, ESI†). The BBB was cleaned through two-step cleaning processes (*i.e.*, activation of gold electrodes and simplified organic cleaning of the device). The activation of gold electrodes was for yielding original gold through the reductive desorption of a gold-thiol SAM, and the organic cleaning was for removing biological remnants (*e.g.*, dead cells during cell loading). These experimental results verify the addressability, multifunctionality, and reusability of the BBB in manipulating cell detachment at a cellular level.

The cell detachment at a subcellular level was also achieved by disconnecting the part of a cell from the BBB having gold lines

with a width of  $10\ \mu\text{m}$  and a gap of  $3\ \mu\text{m}$  (see Fig. 2C). When we activated a gold line on which one end of the cell was placed, the cell was partially detached, and then the detached cytoskeleton finished its retraction within 16 s after subcellular detachment (Fig. 4G). The retraction speed of the detached cytoskeleton at a subcellular level is faster than that of the detached cell at a cellular level because a single cell which has no constraint in stretching itself is under higher tension than confluent cells. Next, the part of NIH 3T3 fibroblasts was detached with a series of activations (Fig. 4H). The second activation (act. 2) was applied 16 s after the first one (act. 1). This experiment reveals that repetitive activations within dozens of seconds do not sacrifice the viability of the cell and are able to gradually increase the amount of subcellular detachment. Together with experimental results for programmable, addressable control of cell adhesion, successful manipulations of subcellular detachment open a possibility for the control of cell motility. In detail, the migration direction of an adherent cell can be controlled by selectively activating some of the gold electrodes of the BBB. When a cell is located on the origin and adheres to 4 gold electrodes that lie in each quadrant, the cell is thought to move in the first quadrant by activating the gold electrode in the third quadrant (or all gold electrodes except the one in the first quadrant). This is because the RGD peptides tethered on inactivated gold electrode(s) have much higher affinity for cell adhesion than bare gold of activated ones.

Finally, we examined the viability of the cells that were adhered/detached to/from the BBB. At first, the effect of an activation potential on the cells adhered on neighboring

extracellular matrix proteins or another cell. (F) Programmable cell patterning using the manipulation of cell detachment on a single four-by-four BBB. The cells are patterned in shapes of “C,” “A,” and “L,” verifying the addressability, multifunctionality, and reusability of the BBB. (G–H) Spatio-temporal manipulation of cell detachment at a subcellular level using the BBB. The part of a NIH 3T3 fibroblast is detached by a single activation (Act. 0). This subcellular detachment is accompanied by the spontaneous retraction of the detached cytoskeleton (G). The part of a cell is sequentially detached by a series of activations (Act. 1 and Act. 2). Scale bars are  $100\ \mu\text{m}$ .

(inactivated) gold electrodes around a target (activated) one was examined. The cells adhered on the neighboring (inactivated) gold electrodes were grown in DMEM supplemented with 10% FBS and 1% Pen-Strep. They reached their confluent stage 96 h after the activation of the target gold electrode, showing their viability (Fig. 5A). The reason for this result is that the cells on the neighboring gold electrodes are electrically disconnected (*i.e.*, floating). Secondly, the viability of the detached cells was characterized by inspecting cell morphology and as well as by using a molecular probe assay kit for cell viability. Two groups of NIH 3T3 fibroblasts, detached from the BBB at activation potentials of  $-1.50$  and  $-1.80$  V respectively, were collected using a centrifuge and then were loaded on a Petri dish. The viability of the two groups was observed 12 h of cell loading. All cells detached at  $-1.50$  V were viable, while about 90% of the cells detached at  $-1.80$  V were still alive rather than electrocuted. The results lay a technical foundation for spatiotemporal manipulation of cell adhesion and detachment with the BBB. Moreover, this shows the maximum activation potential for cell detachment is about  $-1.80$  V (less than  $-2.00$  V).

## Conclusions and future outlook

A biological breadboard has been developed to spatiotemporally manipulate cell adhesion and detachment at cellular and subcellular levels in a programmable, addressable fashion. This platform, composed of identical gold electrodes patterned on a Pyrex substrate, was microfabricated, and then was surface-modified with PEG and RTT. The BBB platform showed the following features: (i) addressability in the manipulation of cell adhesion and detachment due to its structure (*i.e.*, independently operated gold electrodes); (ii) multifunctionality in the characterization of cellular dynamics such as cell positioning, cell patterning, cell motility control, *etc.*; (iii) reusability resulted from the electrochemical reaction of a gold-thiol SAM; (iv) easy incorporation with other conventional instruments. These exquisite features, which have been experimentally demonstrated using NIH 3T3 fibroblasts, present BBB as a robust platform suitable for quantitative characterization of cellular biomechanics. The extrapolation of this technology to other adherent cells is expected to lead to a better understanding of cellular behavior and dynamics.<sup>35,36</sup> Ongoing work is focusing on more in-depth control of cell motility by developing a large-scale BBB to shed light on the dynamics of cell motility. Integrated with subcellular models<sup>36</sup> and molecular dynamics simulations,<sup>37–39</sup> BBB will offer a platform for studies of cell mechanics and mechanotransduction, especially as related to integrin-mediated focal adhesions.<sup>40</sup>

## References

- B. Geiger, A. Bershadsky, R. Pankov and K. M. Yamada, *Nat. Rev. Mol. Cell Biol.*, 2001, **2**, 793–805.
- A. J. Ridley, M. A. Schwartz, K. Burridge, R. A. Firtel, M. H. Ginsberg, G. Borisy, J. T. Parsons and A. R. Horwitz, *Science*, 2003, **302**, 1704–1709.
- T. H. Park and M. L. Shuler, *Biotechnol. Prog.*, 2003, **19**, 243–253.
- P. Clark, P. Connolly, A. S. Curtis, J. A. Dow and C. D. Wilkinson, *Development*, 1987, **99**, 439–448.
- B. Chehroudi, T. R. Gould and D. M. Brunette, *J. Biomed. Mater. Res.*, 1990, **24**, 1203–1219.
- J. W. Lussi, C. Tang, P.-A. Kuenzi, U. Stauffer, G. Csucs, J. Vörös, G. Danuser, J. A. Hubbell and M. Textor, *Nanotechnology*, 2005, **16**, 1781–1786.
- K.-B. Lee, S. J. Park, C. A. Mirkin, J. C. Smith and M. Mrksich, *Science*, 2002, **295**, 1702–1705.
- J. D. Hoff, L.-J. Cheng, E. Meyhöfer, L. J. Guo and A. J. Hunt, *Nano Lett.*, 2004, **4**, 853–857.
- C. S. Chen, M. Mrksich, S. Huang, G. M. Whitesides and D. E. Ingber, *Science*, 1997, **276**, 1425–1428.
- N. Y. Lee, J. R. Lim and Y. S. Kim, *Biosens. Bioelectron.*, 2006, **21**, 2188–2193.
- A. Folch, B. H. Jo, O. Hurtado, D. J. Beebe and M. Toner, *J. Biomed. Mater. Res.*, 2000, **52**, 346–353.
- E. A. Roth, T. Xu, M. Das, C. Gregory, J. J. Hickman and T. Boland, *Biomaterials*, 2004, **25**, 3707–3715.
- A. L. Birkbeck, R. A. Flynn, M. Ozkan, D. Song, M. Gross and S. C. Esener, *Biomed. Microdevices*, 2003, **5**, 47–54.
- M. Ozkan, T. Pisanic, J. Scheel, C. Barlow, S. Esener and S. N. Bhatia, *Langmuir*, 2003, **19**, 1532–1538.
- A. Rosenthal and J. Voldman, *Biophys. J.*, 2005, **88**, 2193–2205.
- J. Lahann, S. Mitragotri, T.-N. Tran, H. Kaido, J. Sundaram, I. S. Choi, S. Hoffer, G. A. Somorjai and R. Langer, *Science*, 2003, **299**, 371–374.
- G. A. Truskey and J. S. Pirone, *J. Biomed. Mater. Res.*, 1990, **24**, 1333–1353.
- T. G. van Kooten, J. M. Schakenraad, H. C. van der Mei, A. Dekker, C. J. Kirkpatrick and H. J. Busscher, *Med. Eng. Phys.*, 1994, **16**, 506–512.
- A. J. García, F. Huber and D. Boettiger, *J. Biol. Chem.*, 1998, **273**, 10988–10993.
- R. S. Cargill, K. C. Dee and S. Malcolm, *Biomaterials*, 1999, **20**, 2417–2425.
- S. C. Kuo and D. A. Lauffenburger, *Biophys. J.*, 1993, **65**, 2191–2200.
- S. C. Kuo, D. A. Hammer and D. A. Lauffenburger, *Biophys. J.*, 1997, **73**, 517–531.
- A. S. Goldstein and P. A. DiMilla, *J. Biomed. Mater. Res.*, 2002, **59**, 665–675.
- D. R. McClay, G. M. Wessel and R. B. Marchase, *Proc. Natl. Acad. Sci. U. S. A.*, 1981, **78**, 4975–4979.
- M. M. Lotz, C. A. Burdsal, H. P. Erickson and D. R. McClay, *J. Cell Biol.*, 1989, **109**, 1795–1805.
- C. A. Burdsal, M. C. Alliegro and D. R. McClay, *Dev. Biol.*, 1991, **144**, 327–334.
- C. A. Burdsal, M. M. Lotz, J. Miller and D. R. McClay, *Dev. Dyn.*, 1994, **201**, 344–353.
- K. L. Sung, L. A. Sung, M. Crimmins, S. J. Burakoff and S. Chien, *Science*, 1986, **234**, 1405–1408.
- E. Evans, K. Ritchie and R. Merkel, *Biophys. J.*, 1995, **68**, 2580–2587.
- J.-Y. Shao and R. M. Hochmuth, *Biophys. J.*, 1996, **71**, 2892–2901.
- R. Inaba, A. Khademhosseini, H. Suzuki and J. Fukuda, *Biomaterials*, 2009, **30**, 3573–9.
- O. Guillaume-Gentil, M. Gabi, M. Zenobi-Wong and J. Vörös, *Biomed. Microdevices*, 2011, **13**, 221–230.
- G. Karp, *Cell and molecular biology: concepts and experiments*, John Wiley & Sons, New York, 2004.
- C. A. Widrig, C. Chunga and M. D. Porter, *J. Electroanal. Chem.*, 1991, **310**, 335–359.
- S.-H. Yoon and M. R. K. Mofrad, *Biomaterials*, 2011, **32**, 7286–7296.
- Y. Jamali, M. Azimi and M. Mofrad, *PLoS One*, 2010, **5**(8), e12097.
- S. Lee, S. Chunsriviro, R. Kamm and M. Mofrad, *Biophys. J.*, 2008, **95**(4), 2027–2036.
- J. Golji and M. Mofrad, *Biophys. J.*, 2010, **99**(4), 1073–1081.
- J. Golji, J. J. Lam and M. Mofrad, *Biophys. J.*, 2011, **100**(2), 332–340.
- M. Mofrad, in *Cellular mechanotransduction: diverse perspectives from molecules to tissues*, ed. R. Kamm, Cambridge University Press, New York, 2010.